modelling

MDPI

Article

Mixing Enhancement Study in Axisymmetric Trapped-Vortex Combustor for Propane, Ammonia and Hydrogen

Heval Serhat Uluk, Sam M. Dakka * and Kuldeep Singh

Faculty of Engineering, University of Nottingham, Campus Park, Nottingham NG7 2RD, UK; heval.uluk@nottingham.ac.uk (H.S.U.); kuldeep.singh@nottingham.ac.uk (K.S.)
* Correspondence: sam.dakka@nottingham.ac.uk; Tel.: +44-115-7486853

Abstract: The trapped-vortex combustor (TVC) is an alternative combustor design to conventional aeroengine combustors. The separate fuel and air injection of this combustor and its compact design make it a perfect candidate for conventional fuel usage. Moreover, the performance of a trapped-vortex combustor with alternative fuels such as ammonia and hydrogen in the actual operating conditions of an aeroengine is not well understood. The present paper focused on the performance evaluation of TVCs with the futuristic fuels ammonia and hydrogen including under the realistic operating conditions of a combustor. The investigated fuels were injected into a cavity with 0-,15-, 30- and 45-degree transverse-angled air injectors to evaluate the mixing enhancement of the air and fuel under idle and low-power conditions. The mixing behavior of hydrogen showed a significant difference from the conventional fuel, i.e., propane. It was also noticed that the transverse injection of the air helped to improve the mixing efficiency as compared to the normal injection configuration. Mixing efficiency was higher for the 30- and 45-degree transverse-angled air injectors compared to the 0- and 15-degree transverse-angled air injectors.

Keywords: aerodynamic; aerospace; computational fluid dynamics; propulsion; trapped-vortex combustor

Citation: Uluk, H.S.; Dakka, S.M.; Singh, K. Mixing Enhancement Study in Axisymmetric Trapped-Vortex Combustor for Propane, Ammonia and Hydrogen. *Modelling* **2024**, *5*, 600–624. https://doi.org/10.3390/modelling5020032

Academic Editors: Kumar K. Tamma and Sergey Utyuzhnikov

Received: 18 March 2024
Revised: 31 May 2024
Accepted: 5 June 2024
Published: 7 June 2024

1. Introduction

Trapped-vortex combustors (TVCs) are combustors that rely on a cavity for flame stabilization, and were designed by HSU et al. [1]. Commercial annular combustors use swirl stabilizers which diverge hot products backwards in the primary zone of combustion process to achieve better fuel–air mixing and establish continuous ignition sources [2–4]. The TVC eliminates the usage of the swirl stabilizer by implementing a cavity inside the combustor. A vortex inside of the cavity is formed and air and fuel are directly injected into the cavity. The direct injection of air and fuel provides control over the equivalence ratio inside the cavity, acting like cooling agents around fuel injectors, and increasing air–fuel mixing [1].

The first-generation trapped-vortex combustor concept was introduced by HSU et al. [1], who were influenced by Little, Whipkey and Mair's [5,6] bluff-body studies. In those studies, they found that bluff body design could reduce the drag in an axisymmetric configuration under atmospheric operating conditions [1,5,6], and they found the lowest drag at a 0.6 cavity aspect ratio [5]. In parallel to this finding, it was also shown that the lowest pressure drop of a trapped-vortex combustor was achievable at a 0.6 cavity aspect ratio [1]. The pressure drop was found to be very small compared to commercial gas turbines, which suggests that the fuel consumption of a well-designed TVC would be very low [1]. Moreover, the lean blow-out limit of the TVC was found to be very low for various operation conditions without disturbing the stability of the vortex, whereas the combustion efficiency was adequate for a wide range [1].

Numerical studies of this model were carried out in [7] for [1,5]. They used Direct Numerical Simulation (DNS) and Reynolds-Averaged Navier–Stokes (RANS) k-ε turbulence models. Even though DNS produced more accurate results than the k-ε turbulence model, it was noted that the k-ε model produced a relatively close result, especially for the optimum cavity aspect ratio of 0.6 [7]. They also stated that the pressure drop was minimum at a 0.6 cavity aspect ratio while vortex shedding occurred at the 0.4 cavity aspect ratio.

Second-generation trapped-vortex combustors involved the first usage of struts with increased temperature and ambient temperature [2]. The struts acted to block incoming air from the mainstream to enhance the mixing of air and fuel, acted as a flameholder, and disturbed the heat between the cavity and main section [2]. Also, the struts heated by combustion acted as an ignition source. The combustion efficiency was slightly improved with the implementation of the struts.

The fuels used for TVCs were gaseous until the invention of third-generation TVCs, for which it was decided that liquid ethanol and jP-8 would be used as fuels [2]. This fuel type was tested under a 650K temperature at atmospheric pressure. The design of the combustor was similar to second-generation combustors, and in this experiment, the effect of the fuel injection location was evaluated. It was found that injection locations that produced a double vortex inside the cavity increased combustion efficiency, and showed the lowest lean blow-out limit.

Since these combustors will be used in the aviation sector, it was necessary to test this new concept under realistic conditions. The performance of the TVC under realistic operating conditions (high temperature and high pressure) was evaluated with the fourth TVC concept. The combustion efficiency was over 99%, the lean blow-out limit was 50% lower than commercial gas turbines and the relight capacity of the TVC was superior to conventional gas turbines under a wide range of operating conditions [2].

TVCs were tested using various fuels in the literature, which is good proof that they are valid candidates for future combustors. Methane, hydrogen and propane are the most common ones that are tested in TVCs [1,2,8–10]. Another alternative fuel biogas was also tested in TVCs [11], and ethanol is another alternative fuel that was used in this new combustor concept [2,12]. Recently, hydrogen fuel was tested in a trapped-vortex combustor that generates a vortex aerodynamically instead of geometrically [13]. It is further stated that fuel that contains 65% hydrogen by volume is able to burn in this combustor with low NO_X emissions without diluting the fuel blend [13,14].

Recently, when hydrogen-fueled TVCs that contained a swirling motion inside the cavity were investigated by [15] using large eddy simulations, it was found that a swirling motion was able to decrease pressure fluctuations when combustion occurred. Even though increasing the swirl caused NO emissions to rise, the number was still at an acceptable level, and the combustion efficiency reached around 99.8%. Another novel approach was also tested experimentally by [16]. Their findings suggest that swirling TVCs can enhance the combustion efficiency under different operating conditions; their temperature distributions at the outlet can be improved with the swirl effect and their emission levels are promising. Another approach to using TVCs is using a mixed flow, where the cavity acts as a pilot stage for flame stabilization and works alone under low-power conditions, and the fuel is also introduced at the main stage when the engine operates under high-power conditions [17]. Mixed-flow TVCs were tested numerically and experimentally by [18]. Their focus was mainly on temperature distribution at the outlet area; they noted that the temperature reached its peak just above the middle of the outlet section, which meets the design requirements of a combustor. The cooling of mixed-flow TVCs was investigated by [17], but they observed that the cooling design was not efficient because of the lack of a liner wall which made it difficult to apply the film-cooling layer. Another approach to altering combustion characteristics was achieved by implementing a wave rotor before a trapped-vortex combustor by [19]. They stated that a stable flame forms under a low wave rotor speed, and the flame becomes unstable when the rotor uses its 85% capacity. TVCs are

also used in scramjet applications. Recently, a scramjet fueled with hydrogen was tested numerically with a detached eddy simulation by [20], and their conclusion was that the combustion instabilities and shockwaves stemmed from the combustion mode rather than the equivalence ratios.

Scope of Current Work

The novelty of the current work compared to previous work is that the current configuration is optimized for a variety of fuels as compared with previous work, where it was optimized for propane and methane.

In this study, the design of a trapped-vortex combustor which works under actual operating conditions [1] will be used and improved in terms of air–fuel mixing. This study firstly introduces transverse injection angles to observe mixing efficiency. The simulation will be performed under realistic conditions as in fourth-generation TVCs to prove that it is suitable for aviation applications. The final objective of this paper is to test alternative fuels in this newfound combustor design. Propane, hydrogen and ammonia will be compared in terms of air–fuel mixing with the new fuel injection locations. The most crucial aspects of this study are that the usage of transverse angled air injection in this design improves mixing efficiency and that alternative fuels are used in the TVC to evaluate their suitability under realistic operating conditions.

2. Materials and Methods

2.1. Geometry

The combustors that are shown in Figures 1 and 2 are identical to the domains that were used in [1,21]. The air injectors in the present study were transverse-angled, and the fuel injectors remained normal to the afterbody. Two bluff bodies were used to form a cavity, and propane was chosen for the axisymmetric trapped-vortex combustor (Figure 1). A spindle, which had a 9 mm diameter, connected these two bluff bodies, and air and fuel injection pipes were placed inside of it. Propane was injected inside the cavity with 8 fuel injectors that were surrounded by 24 air injectors (Figure 2). The afterbody could be moved along the spindle to change the cavity length (L_{ca}), and hence the cavity aspect ratio. The combustor's overall diameter was 80 mm, where the main inlet section had a fore body diameter of 70 mm (d_f), and the cavity was created by placing an afterbody that had a 50.8 mm dimeter [1]. The geometry dimensions of axisymmetric trapped-vortex combustor is illustrated in Table 1.

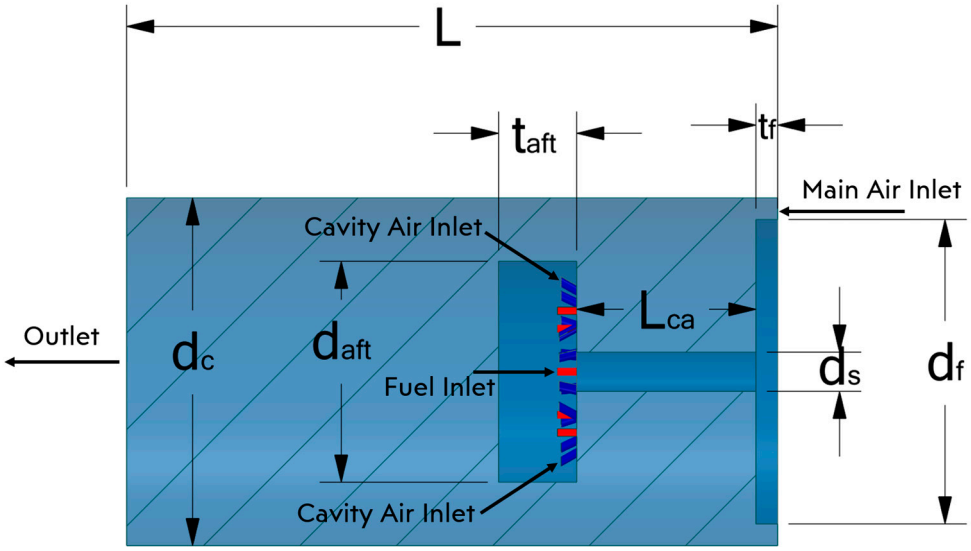

Figure 1. Side view of axisymmetric trapped-vortex combustor adopted from [1].

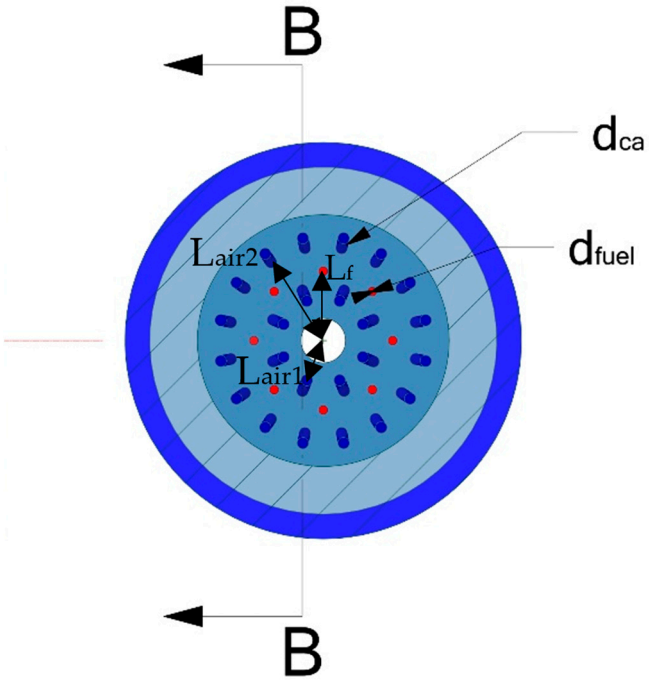

Figure 2. Cavity injection points of axisymmetric trapped-vortex combustor adopted from [1].

Table 1. Geometry dimensions of axisymmetric trapped-vortex combustor [1,21].

Parameters	Values (mm)
Combustor Length, L	150
Forebody Diameter, d_f	70
Combustor Diameter, d_c	80
Afterbody Diameter, d_{aft}	50.8
Spindle Diameter, d_s	9
Cavity Length, L_{ca}	41.3
Fuel Injection Diameter, dfuel	1.75
Cavity Injection Diameter, d_{ca}	2.29
Distance of Inner Cavity Air Injection, L_{air1}	11
Distance of Outer Cavity Air Injection, L_{air2}	19
Distance of Fuel Injection, L_t	14
Thickness of Afterbody, t_{aft}	18
Thickness of Forebody, t_f	5

2.2. Governing Equations

The equations used to the solve RANS k-ε Realizable model are defined as follows [21,22]:
Continuity Equation:

$$\frac{\delta \rho}{\delta t} + \frac{\delta}{\delta x_i}(\rho \overline{u}_i) = 0 \quad (1)$$

Momentum Equation:

$$\frac{\delta}{\delta t}(\rho \overline{u}_i) + \frac{\delta}{\delta x_j}(\rho \overline{u}_i \overline{u}_j) = \frac{\delta}{\delta x_j}(\sigma_{ij}) - \frac{\delta \overline{p}}{dx_i} - \frac{\delta \tau_{ij}}{\delta x_j} \quad (2)$$

σ_{ij} is the stress tensor generated by molecular viscosity,

$$\sigma_{ij} = \left[\mu\left(\frac{\delta \overline{u}_i}{\delta x_j} + \frac{\delta \overline{u}_j}{\delta x_i}\right)\right] - \frac{2}{3}\mu \frac{\delta \overline{u}_l}{\delta x_l}\delta_{ij} \quad (3)$$

and $\delta\tau_{ij}$ is the subgrid-scale stress, which can be calculated as

$$\tau_{ij} \equiv \rho\overline{u_i u_j} - \rho\overline{u}_i\overline{u}_j \tag{4}$$

The transport equation of k is written as:

$$\frac{\delta}{\delta t}(\rho k) + \frac{\delta}{\delta x_j}(\rho k u_j) = \frac{\delta}{\delta x_j}\left[(\mu + \frac{\mu_t}{\sigma_k})\frac{\delta_k}{\delta x_j}\right] + G_k + G_b - \rho\varepsilon - Y_M + S_k \tag{5}$$

G_k is the turbulence kinetic energy from the mean velocity gradient, whereas G_b is the turbulence kinetic energy from buoyancy. Y_M is the addition of fluctuating dilation in compressible turbulence to overall dissipation.

$$G_k = \mu_t S^2 \tag{6}$$

$$S = \sqrt{2S_{ij}S_{ij}} \tag{7}$$

$$S_{ij} = \frac{1}{2}(\frac{\delta u_j}{\delta x_i} + \frac{\delta u_i}{\delta x_j}) \tag{8}$$

$$G_b = -g\frac{\mu_t}{i\rho Pr_t}\frac{\delta p}{\delta x_i} \tag{9}$$

μ_t is the turbulence viscosity, S is the modulus of the mean rate-of-strain tensor, Pr_t is the turbulent Prandtl number and g is the gravity, while the transport equation of ε can be expressed as:

$$\frac{\delta}{\delta t}(\rho\varepsilon)\frac{\delta}{\delta x_j}(\rho\varepsilon u_j) = \frac{\delta}{\delta x_j}\left[(\mu + \frac{\mu_t}{\sigma_\varepsilon})\frac{\delta_\varepsilon}{\delta x_j}\right] + \rho C_1 S\varepsilon - \rho C_2\frac{\varepsilon^2}{k + \sqrt{\nu\varepsilon}} + C_{1\varepsilon}\frac{\varepsilon}{k}C_{3\varepsilon}G_b + S_\varepsilon \tag{10}$$

σ_k and σ_ε are the Prandtl numbers for k and ε while S_k and S_ε are the user-defined source terms. C_1 is calculated with Equations (11) and (12):

$$C_1 = max\left[0.43,\ \frac{\eta}{\eta + 5}\right] \tag{11}$$

$$\eta = S\frac{k}{\varepsilon} \tag{12}$$

The other model constants are as follows by default:

$$C_1 = 1.44\ ,\ C_2 = 1.9\ ,\ \sigma_k = 1, \sigma_\varepsilon = 1.2$$

Turbulent viscosity (μ_t) can be calculated with Equations (13)–(17):

$$\mu_t = qC_\mu\frac{k^2}{\varepsilon} \tag{13}$$

$$C_\mu = \frac{1}{A_0 + A_S\frac{kU^*}{\varepsilon}} \tag{14}$$

$$U^* = \sqrt{S_{ij}S_{ij} + \widetilde{\Omega}_{ij}\widetilde{\Omega}_{ij}} \tag{15}$$

$$\widetilde{\Omega}_{ij} = \Omega_{ij} - 2\varepsilon_{ijk}\omega_k \tag{16}$$

$$\Omega_{ij} = \overline{\Omega}_{ij} - \varepsilon_{ijk}\omega_k \tag{17}$$

$\overline{\Omega}_{ij}$ is the mean rate-of-rotation tensor, where A_0 = 4.04 and A_S is calculated as:

$$A_S = \sqrt{6}\sin\varphi \tag{18}$$

$$\varphi = \frac{1}{3}\cos^{-1}\left(\sqrt{6W}\right) \tag{19}$$

$$W = \frac{S_{ij}S_{jk}S_{ki}}{\tilde{S}^3} \tag{20}$$

After the species transport model was applied to the simulation, the software predicted the local mass fraction for all of the species (Y_i). The conservation equation was altered to Equation (21).

$$\frac{\delta}{\delta t}(\rho Y_i) + \nabla\cdot\left(\rho\vec{v}Y_i\right) = -\nabla\cdot\vec{J}_i + R_i + S_i \tag{21}$$

where R_i represents the net production of species, S_i stands for the rate of creation by addition from the dispersed phase and user-defined sources.

The diffusion flux of species ($\vec{J}_i$) is calculated by using Fick's law for turbulent flows as follows:

$$\vec{J}_i = -\left(\rho D_{i,m} + \frac{\mu_t}{Sc_t}\right)\nabla Y - D_{T,i}\frac{\nabla T}{T} \tag{22}$$

in which Sc_t is the turbulent Schmidt number, the default number of which is 0.7. μ_t is the turbulent viscosity, and D_t is the turbulent diffusivity.

$$Sc_t = \frac{\mu_t}{\rho D_t} \tag{23}$$

The transport of the enthalpy that stems from the species diffusion is calculated as:

$$\left[\sum_{i=1}^{n} = h_i\vec{J}_i\right] \tag{24}$$

2.3. Solution Procudure

The simulations were run using ANSYS Fluent 21.1.0. The Reynolds-Averaged Navier–Stokes (RANS) k-ε Realizable model with a standard wall function was used to model the turbulence inside the combustor. The RANS k-ε Realizable model is a very common turbulence model in this research area [23–29]. The turbulence model was also used in the application that used ammonia and hydrogen as fuels [30,31]. It was also stated that the k-ε Realizable model is superior to the k-ω Shear Stress Model (SST) and the k-ω standard in terms of capturing results and computational efficiency [31]. However, the above is true for subsonic speeds; for high-speed airbreathing engines such as ramjets and scramjets, large eddy simulations, which are a compromise between RANS and DNS, are recommended due to computational time constraints [32]. This entails resolving larger turbulent scales than grid spacing while subgrid scales and their impacts on larger grid scales are modeled, enabling the flow physics of transient phenomena such as shock–shock and shock-to-boundary layer and turbulence chemistry interactions to be captured. For locking the flame inside the cavity, enhancing fuel–air mixing, and hence improving combustor performance characteristics, the location of the direct fuel injection into the cavity demonstrated superior performance on the back wall of the cavity as compared to the front wall and farther away from the mainstream combustor inlet [33]. The PISO algorithm was used for pressure–velocity coupling [4,34], and governing equations were discretized by using the Quadratic Upstream Interpolation for Convective Kinematics (QUICK) scheme [25,35], whereas the pressure terms were discretized by using the Pressure-Staggering Option (PRESTO) Scheme [35]. The solution was run until 5.10^{-5} convergence criteria met.

The species transport model was used for creating fuel mixture and energy equations. The one-step reaction mechanism that is embedded in ANSYS software 21.1.0 was used for the propane (Equation (1)) and hydrogen (Equation (2)) fuels. However, the San Diego mechanism was adopted from an online source, shared in the Data Availability Statement section, and used for the ammonia fuel [36].

$$C_3H_8 + 5O_2 \rightarrow 3CO_2 + 4H_2O \tag{25}$$

$$H_2 + \frac{1}{2}O_2 \rightarrow H_2O \tag{26}$$

2.4. Boundary Conditions

Only air was injected at the main air inlet area, whereas air and fuel were injected into the cavity at separate injection locations that were placed at the afterbody, and the outlet area was located downstream of the TVC (Figure 1). The velocity inlet boundary conditions were the main air inlet, cavity air inlet, and fuel inlet sections, and the outlet condition was the pressure outlet. The fuel mass fraction and temperature of incoming air were set for each boundary. Cavity walls were defined with adiabatic and no-slip conditions. The operating conditions of pressure and temperature were set for each case. Table 2 shows the boundary conditions of the cases that are numerically solved in this paper.

Table 2. Boundary conditions for axisymmetric trapped-vortex combustor.

Case	Main Air Velocity (m/s)	Fuel Velocity (m/s)	Injection Air Velocity (m/s)	Transverse Air Injection Angle	Lateral Air Injection Angle	Operating Condition Temperature (K)	Fuel Type
Case 1	42	22	10	0	0	375	Propane
Case 2	42	22	10	15	0	375	Propane
Case 3	42	22	10	30	0	375	Propane
Case 4	42	22	10	45	0	375	Propane
Case 5	42	22	10	0	0	500	Propane
Case 6	42	22	10	15	0	500	Propane
Case 7	42	22	10	30	0	500	Propane
Case 8	42	22	10	45	0	500	Propane
Case 9	42	22	10	0	0	375	Hydrogen
Case 10	42	22	10	15	0	375	Hydrogen
Case 11	42	22	10	30	0	375	Hydrogen
Case 12	42	22	10	45	0	375	Hydrogen
Case 13	42	22	10	0	0	375	Ammonia
Case 14	42	22	10	15	0	375	Ammonia
Case 15	42	22	10	30	0	375	Ammonia
Case 16	42	22	10	45	0	375	Ammonia

2.5. Grid-Independence Study

A three-dimensional poly-hexahedral mesh approach was used for the meshing of axisymmetric TVCs with the fluent meshing tool that comes with ANSYS (Figure 3). The surface mesh was created with poly meshes whereas the volume mesh was discretized with hexahedral meshes. Half of the actual domain was used to reduce the computation cost. The mesh number increased around 1.5 times for each case to make the solution grid independent as per the recommendation of [37]. Four meshes with the cell counts of 2.97 million, 3.5 million, 4.69 million, and 6.95 million were used for this study, this is illustrated in Table 3. Since this paper focuses on non-reacting simulations, total pressure and velocity gradient are important criteria to solidify grid independence.

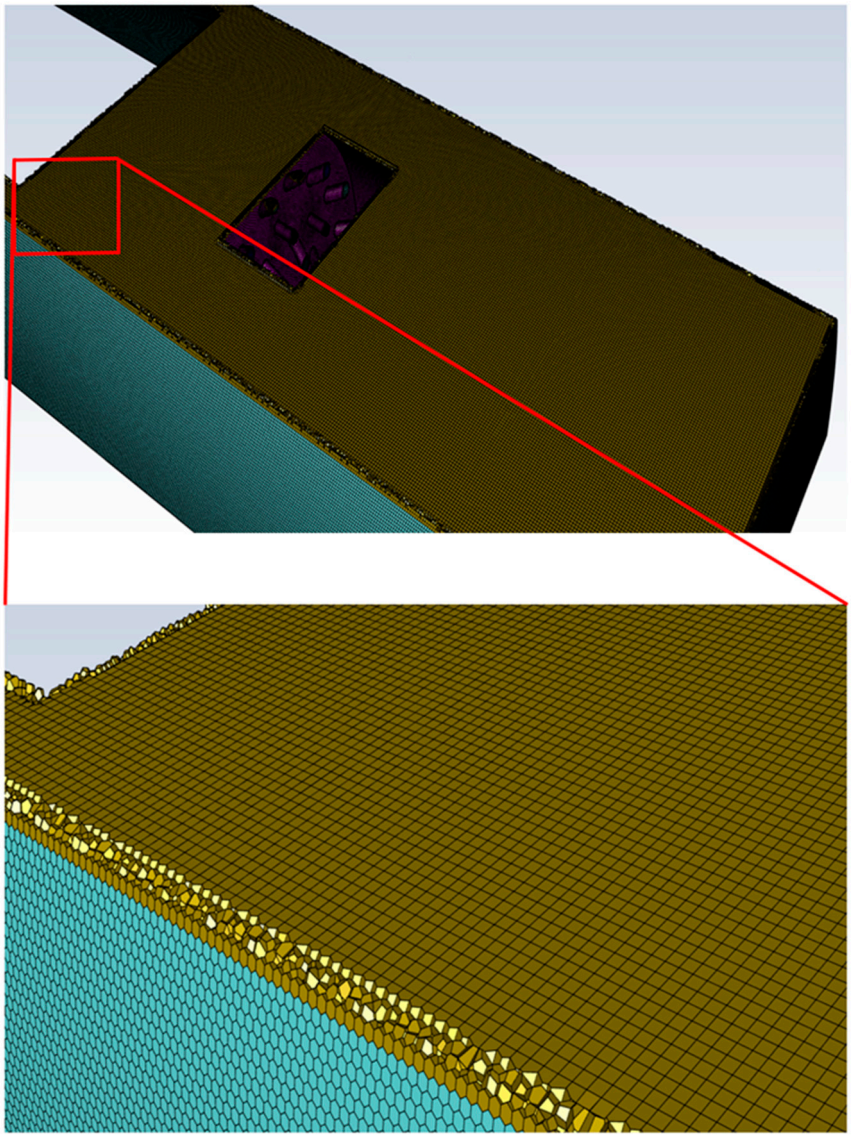

Figure 3. Poly-hexahedral mesh.

Table 3. Grid-independence study for axisymmetric TVC.

Abbreviation	Dimension
Mesh Number 1	2,970,000
Mesh Number 2	3,500,000
Mesh Number 3	4,690,000
Mesh Number 4	6,950,000

Total pressure drops and velocity magnitude inside the cavity at x = 0.036 were observed. It was found that mesh number 3 generated a high total pressure at y = 0.038, whereas mesh number 2 produced a high total pressure at y = 0.014 (see Figure 4) compared with the results for mesh number 4. A similar trend can be seen in Figure 5 for velocity magnitude. Nevertheless, the predicted pressure dropped, and the velocity distributions of mesh number 3 and mesh number 4 were identical. On an average, a difference of 0.1% was observed in the prediction of critical parameters using mesh number 3 and mesh number 4. Finally, mesh number 3 was selected for further study as it was computationally efficient as compared to mesh number 2, and as accurate as the predictions of mesh number 4.

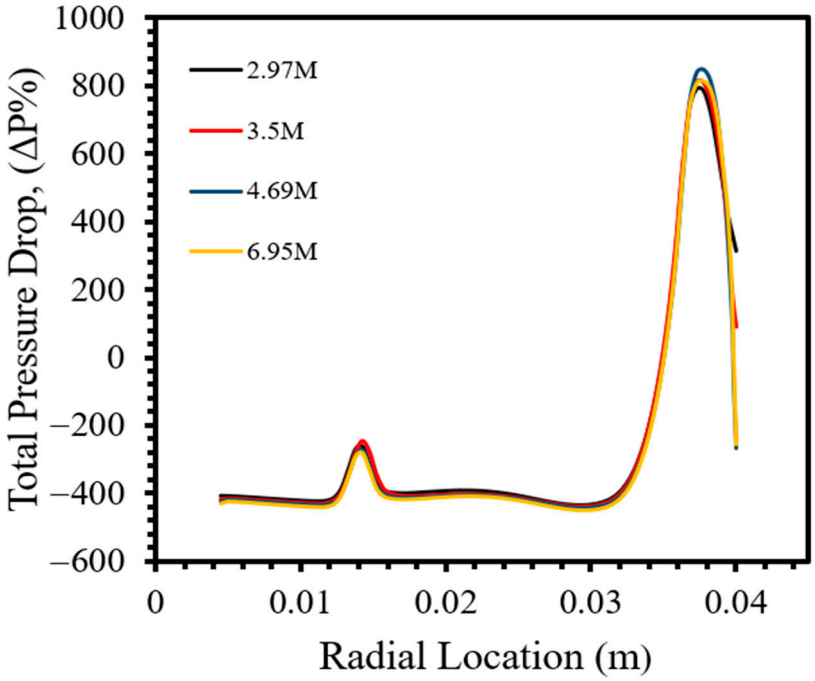

Figure 4. Grid-independence study for total pressure drop at x = 9 mm.

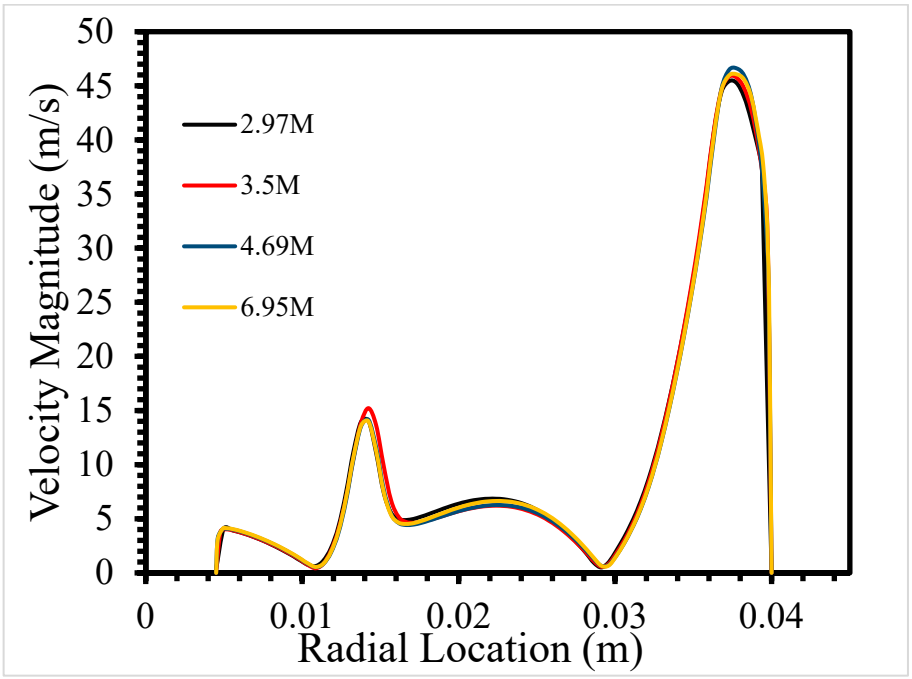

Figure 5. Grid-independence study for total pressure drop at x = 9 mm.

2.6. Validation Study

The domain used for the validation study was adopted from [1], and the geometrical features of it are described in detail in Section 2.1. They were successfully able to measure radial temperature via Coherent Anti-Stokes Raman Spectroscopy, and static pressure drop by implementing a water manometer [1]. Since the scope of this study is non-reacting flow, the only used parameter in our validation study was pressure drop percentage, which is a very crucial parameter for combustor design. The validation study was conducted for the cavity aspect ratios of 0.3, 0.6 and 1 for the main air velocities of 14 m/s, 28 m/s and 42 m/s. The fuel and air injectors were turned off for the validation study, as was

the case in the experiment in [1]. Figure 6 demonstrates the results of the simulations for all velocities and cavity aspect ratios, with the error compared to the HSU experiment. The lowest total pressure drop was observed at the 0.6 cavity aspect ratio for all main air inlet velocities, which was similar to the experiment (see Figure 6). Total pressure drops increased with an increase in the main air velocity. The total pressure drops decreased as the cavity aspect ratio got closer to the optimum cavity length, which was 0.6 according to the experiment and the numerical study. The findings of the numerical study showed that the k-ε Realizable model with a standard wall function could capture the turbulence fluctuations inside the cavity and generate good results.

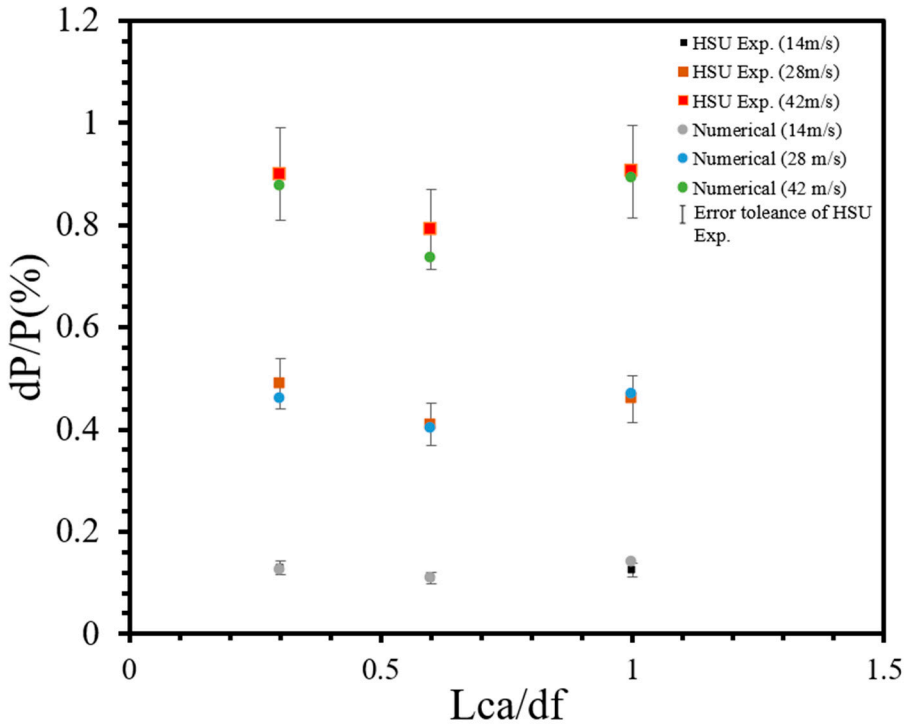

Figure 6. Total pressure drop percentage for the cavity aspect ratios of 0.3, 0.6 and 1 for the 14 m/s, 28 m/s and 42 m/s main air inlet velocities.

3. Results and Discussion

The propane fuel was firstly evaluated under idle and low-power operating conditions for 0, 15-, 30- and 45-degree transverse-angled air injectors. The reason why air injectors with higher transverse angles were not used is that the mixing point of air and fuel would be too close to the fuel injectors. A high air–fuel concentration near the fuel inlet could damage the fuel injector when ignition occurs. After that, ammonia and hydrogen were tested in the operating conditions that was decided in the previous sections for the 0-, 15-, 30- and 45-degree transverse-angled air injectors. The evaluation was conducted by comparing the mixing efficiency and mass fraction distribution of fuel.

3.1. Impact of Transverse Injection Angle for Propane under Idle and Low-Power Conditions

The impact of transverse injection was investigated under two realistic gas turbine operating conditions [38] (see Table 2). The air injectors were angled in the transverse direction whereas the fuel injectors were kept at 0 degrees, normal to the afterbody, for all cases (see Figure 7). Four different transverse air injector angles were used (0, 15, 30 and 45 degrees).

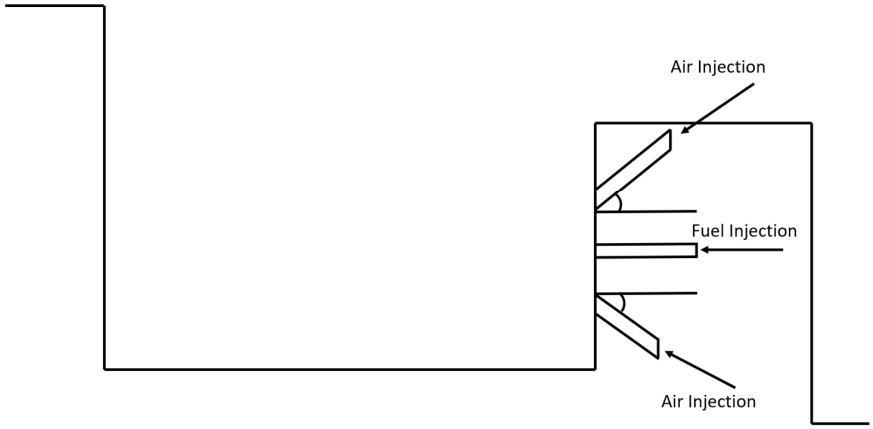

Figure 7. Air and fuel injector alignment.

The mixing of air and fuel was evaluated by using the mixing efficiency definitions of Equations (27) and (28), which are adopted from [39]:

$$\eta_{mix} = \iint Y^{r}_{C_3H_8} \rho u . d_y d_z \Big/ \iint Y_{C_3H_8} \rho u . d_y d_z \tag{27}$$

$$Y^{r}_{C_3H_8} = \begin{cases} Y_{C_3H_8}, \; Y_{C_3H_8} < Y^{st}_{C_3H_8} \\ Y^{st}_{C_3H_8} \left(\frac{1 - Y_{C_3H_8}}{1 - Y^{st}_{C_3H_8}} \right), Y_{C_3H_8} > Y^{st}_{C_3H_8} \end{cases} \tag{28}$$

The fuel and air injectors were located inside the cavity at $X/d_f = 0.671$. It is evident that η_{mix} was high for the 0-degree angled air injectors, and the mixing efficiency decreased downstream of the fuel injection. The highest efficiencies were near the fuel injectors at 0, 15 and 45 degrees; the only exception for this was 30 degrees, which had the lowest $\eta_{mix} = 0.26$ at $X/d_f = 0.642$. The 0- and 45-degree-angled air injectors showed a similar trend, and the only difference was that the 45-degree-angled air injector had a better η_{mix} overall (see Figure 8). The highest mixing efficiency was 0.3 for 45 degrees near the fuel injector location. The mixing efficiency near the fuel injector location should be lower because a high mixing efficiency near the fuel inlet would cause high temperatures at this location. The incoming fuel would immediately burn before it would be able to mix with air inside the cavity. Moreover, a high-temperature flame could propagate inside the fuel injectors, which would damage the injectors.

The η_{mix} value was slightly lowered as the fuel moved towards the forebody between $X/d_f = 0.214$ and $X/d_f = 0.428$, which suggests that the presence of the vortex center in this location had a great influence on η_{mix} and neglected the effect of the air injection transverse angle, but the 45-degree-angled injectors showed relatively better η_{mix} at this location. The lowest η_{mix} was achieved with the 0-degree-angled air injectors downstream of the fuel injectors, which suggests that it provides lower air–fuel mixing at this area. The 15- and 45-degree air injectors had slightly better mixing compared to the 0-degree injectors, but the 30-degree air injector had superior η_{mix} at the end of the cavity. The main reason for this is that at 30 degrees, the fuel moves towards the lower vortex and this unburnt fuel can reach the end of the cavity. It is evident that the 30-degree-angled transverse air injector changed the trajectory of the fuel injection (see Figure 9). While the fuel injection concentration is high around $Y/d_f = 0.17$ for the 0-degree and 45-degree injectirs, there is more fuel observed even at $Y/d_f = 0.15$ and $Y/d_f = 0.13$ for the 15-degree and 30-degree angles, respectively. Moreover, Figure 10 supports the mixing efficiency study, as the fuel concentration at the bottom of the cavity is much higher for the 30-degree-angled air injector. The change in the trajectory of the fuel injection allows more fuel to move towards the bottom of the cavity, and hence it increases mixing efficiency at the end of the cavity. This is important because the main purpose of the usage of the trapped-vortex concept is that it is desirable to be able to diffuse fuel inside the cavity equally to create a more sustainable flame.

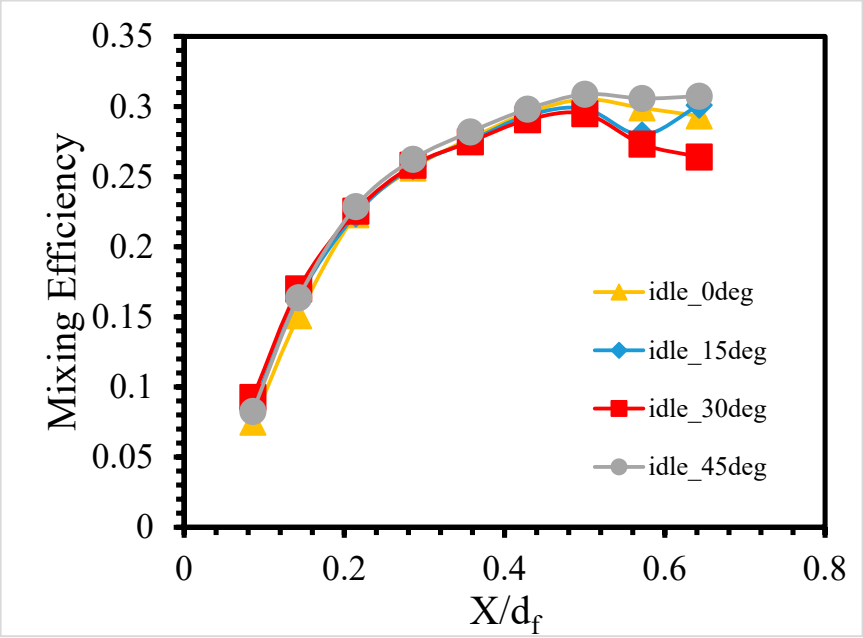

Figure 8. Mixing efficiency inside cavity for idle operating condition for propane.

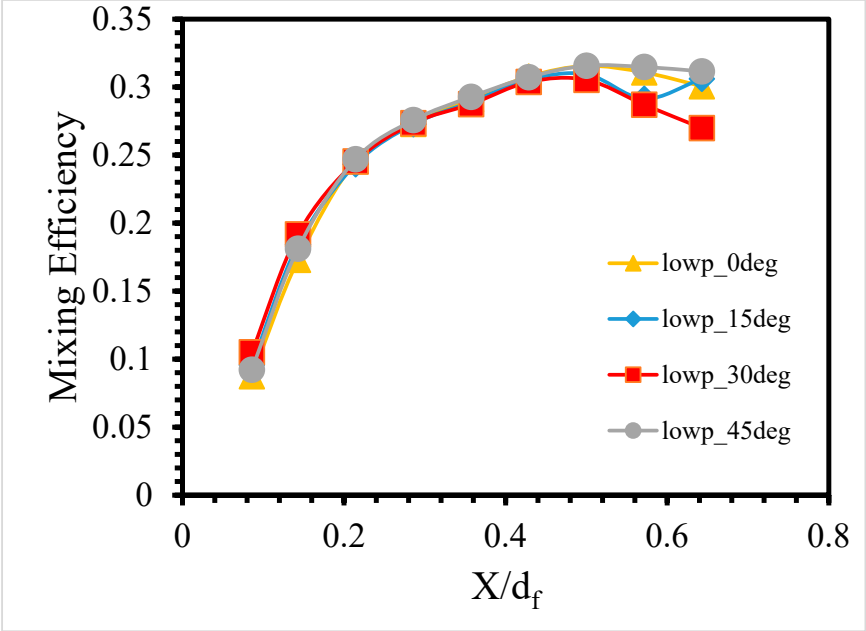

Figure 9. Mixing efficiency inside cavity for low-power operating condition for propane.

After changing the operating conditions to a low-power setup, the mixing efficiency for all points increased slightly because the increased pressure inside the cavity increased the velocity (see Figure 9). There was no significant difference between trends for the idle and lo power operating conditions, but the trends of the 30-degree angle became more significant. While the mixing efficiency at the inlet measured much lower than the other angles compared to idle operating conditions, the η_{mix} of the 30-degree angle became higher downstream of the cavity at $X/d_f = 0.142$ and $X/d_f = 0.085$. Therefore, it can be concluded that 30-degree transverse-angled air injectors distribute fuel inside the cavity more equally, prevent overheating around the fuel injectors, and show rising effectiveness with realistic operating conditions. The other important point about our results is the sudden drop at X/df = 0.571 for the 15-degree transverse-angle air injector under both operating conditions. This decrease stems from the lack of fuel presence at the lower vortex, and X/df = 0.571 goes

through this vortex's center, which causes a sudden drop. Figure 10 represents the mass fraction of propane with streamlines inside the cavity. It is evident that the low-power condition's mass fraction of the propane is higher than that of the idle power condition (Figure 11). When the idle condition has a mass fraction of propane of around 0.2–0.35 for all air injector angles, this figure goes up to 0.3–0.4 for the low-power condition, reinforcing the argument of increasing mixing efficiency as the operating conditions become more realistic.

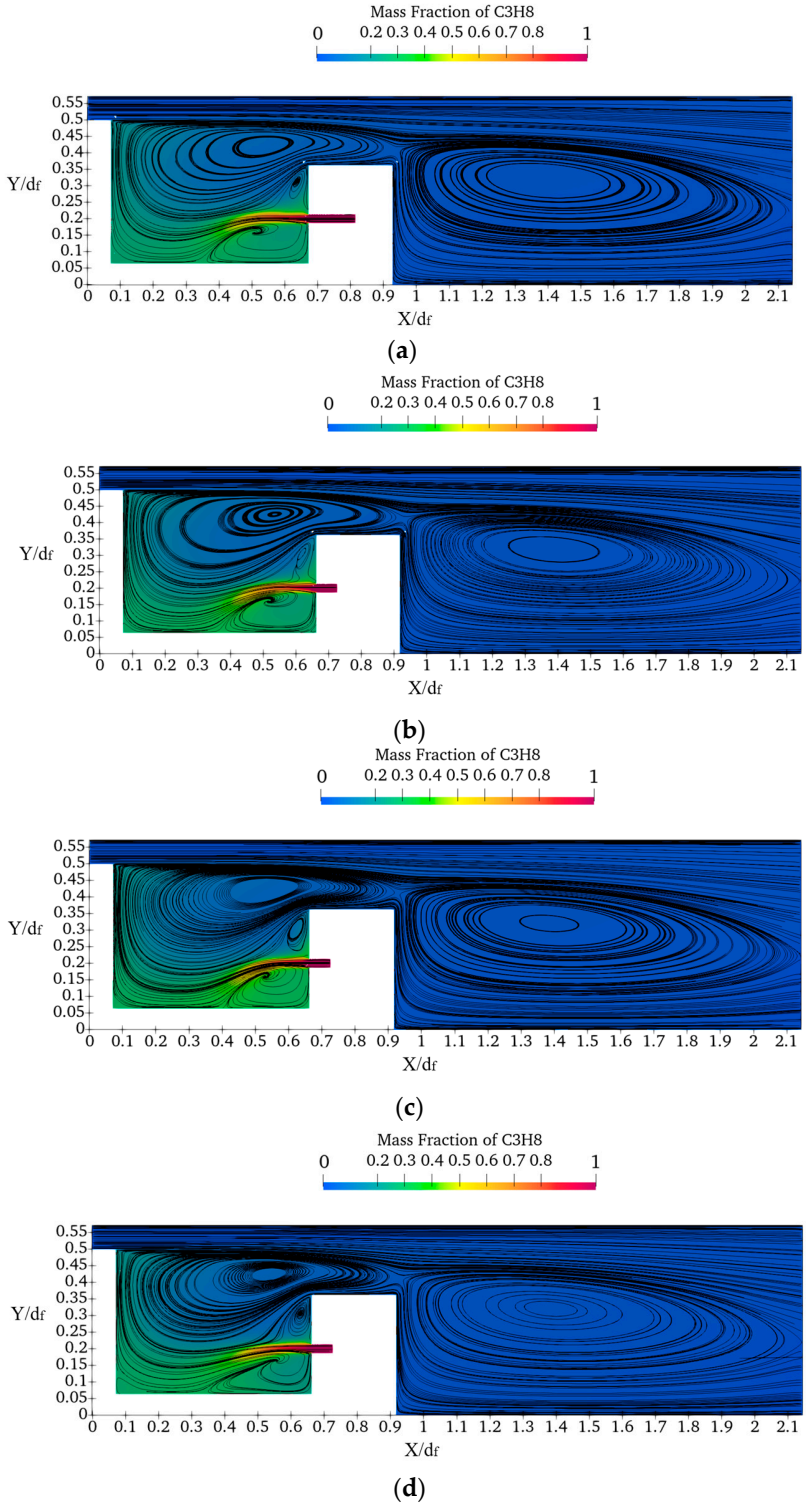

Figure 10. Mass fraction of propane with streamlines under idle operating condition for (**a**) 0-degree, (**b**) 15-degree, (**c**) 30-degree and (**d**) 45-degree angles.

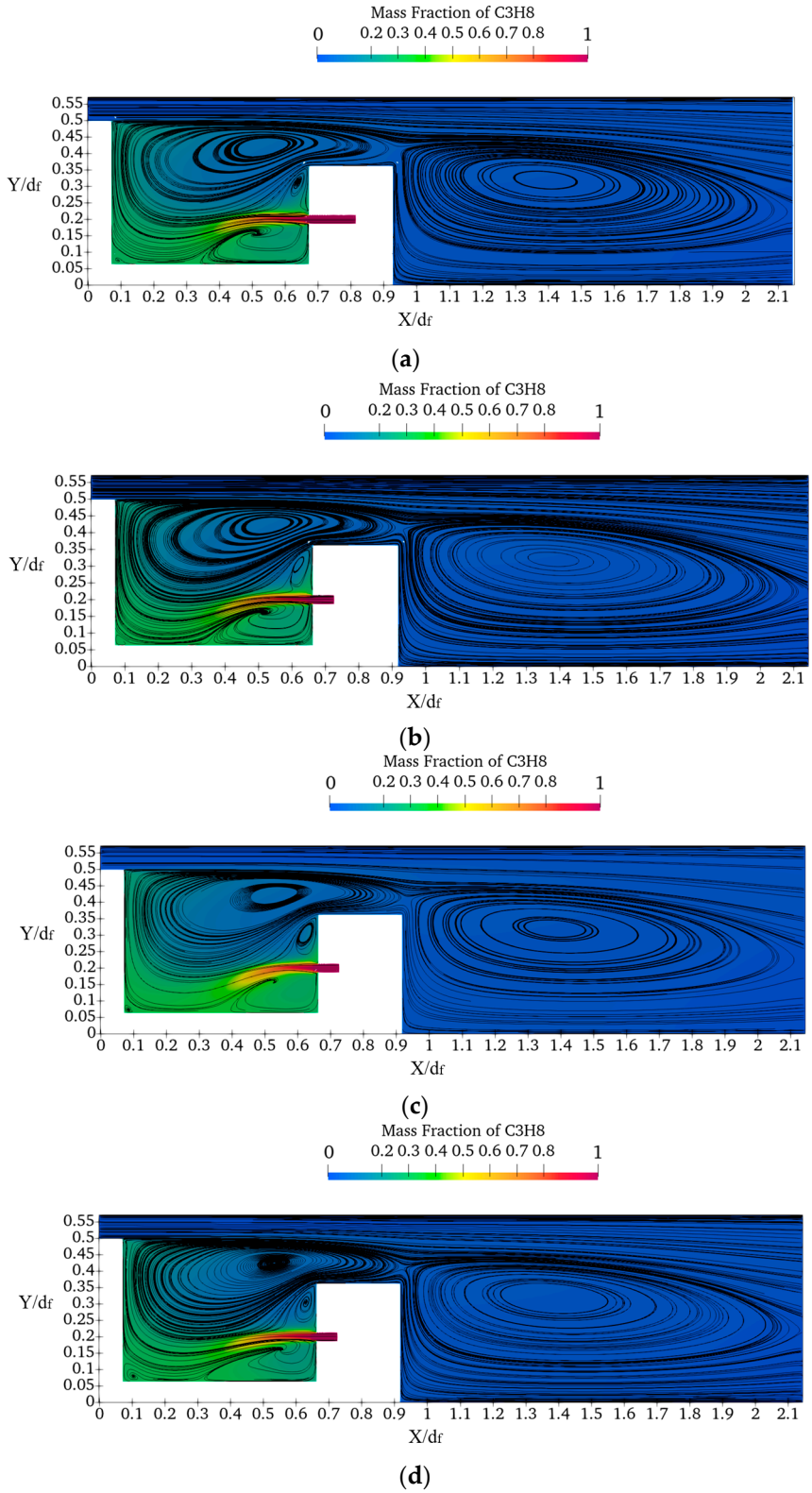

Figure 11. Mass fraction of propane with streamlines under low-power operating condition for (**a**) 0-degree, (**b**) 15-degree, (**c**) 30-degree and (**d**) 45-degree angles.

3.2. Mixing Enhancement of Fuel and Air for Hydrogen and Ammonia

A mixing enhancement study was further conducted for pure hydrogen and ammonia fuels. Both fuels were tested at four different transverse angles (0, 15, 30 and 45 degrees) under the idle condition. The cases 9–12 used for the hydrogen fuel are shown in Figure 12.

It is found that the mixing efficiency overall is lowered compared with the other fuels tested, and the differences in mixing efficiency around the fuel jets and the end of the cavity were specifically low compared to the propane and ammonia fuels. While the lowest η_{mix} was 0.25 for propane around fuel jets, the measured highest η_{mix} was only 0.23 for hydrogen (see Figure 12). The high diffusivity of hydrogen allows it to diffuse immediately inside the cavity, and therefore the mixing efficiency of hydrogen was the lowest throughout the cavity compared to propane and ammonia. Figure 13 shows that the hydrogen concentration is mainly diffused at the top side of the fuel injection side; this is the reason why the mixing efficiency was lower compared to the other fuels. However, it is observed that as the air injector angle increased, the trajectory of the fuel injection moved towards the inside of the cavity, which is the reason why the 45-degree-angled air injector configuration was found to have the highest mixing efficiency. Due to this fact, it can be argued that the trapped-vortex combustor needs some alterations to enhance hydrogen fuel mixing more efficiently.

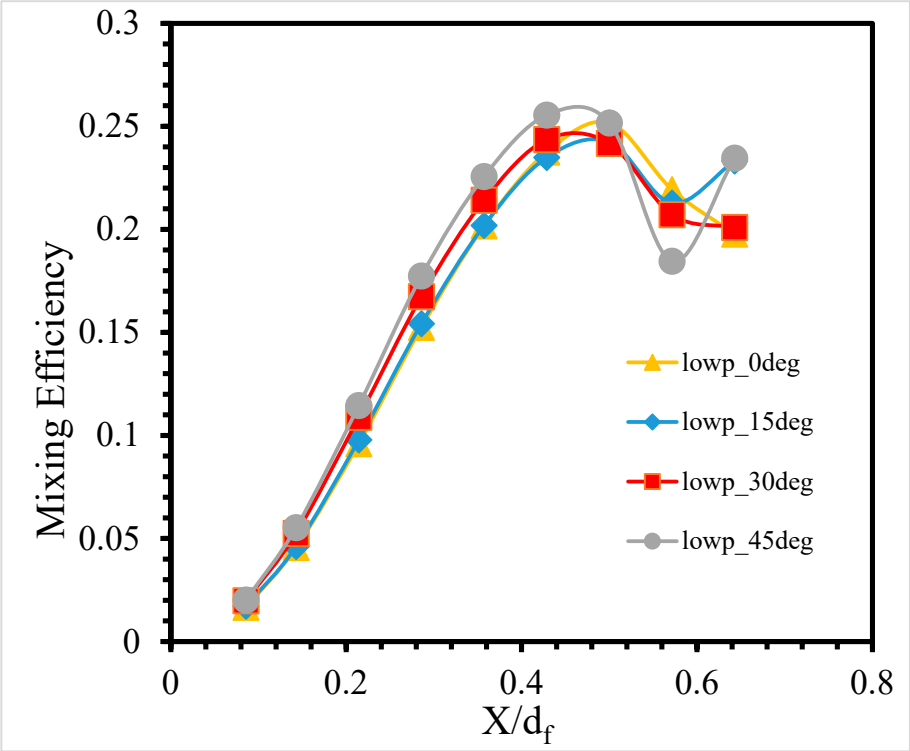

Figure 12. Mixing efficiency inside cavity for idle operating condition for hydrogen.

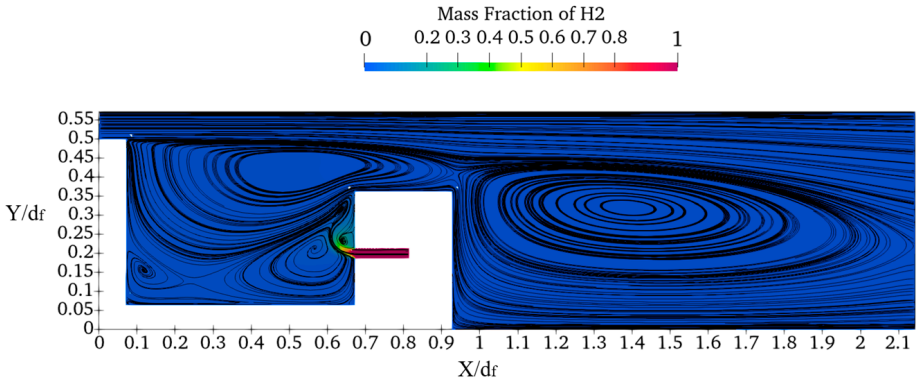

(**a**)

Figure 13. *Cont.*

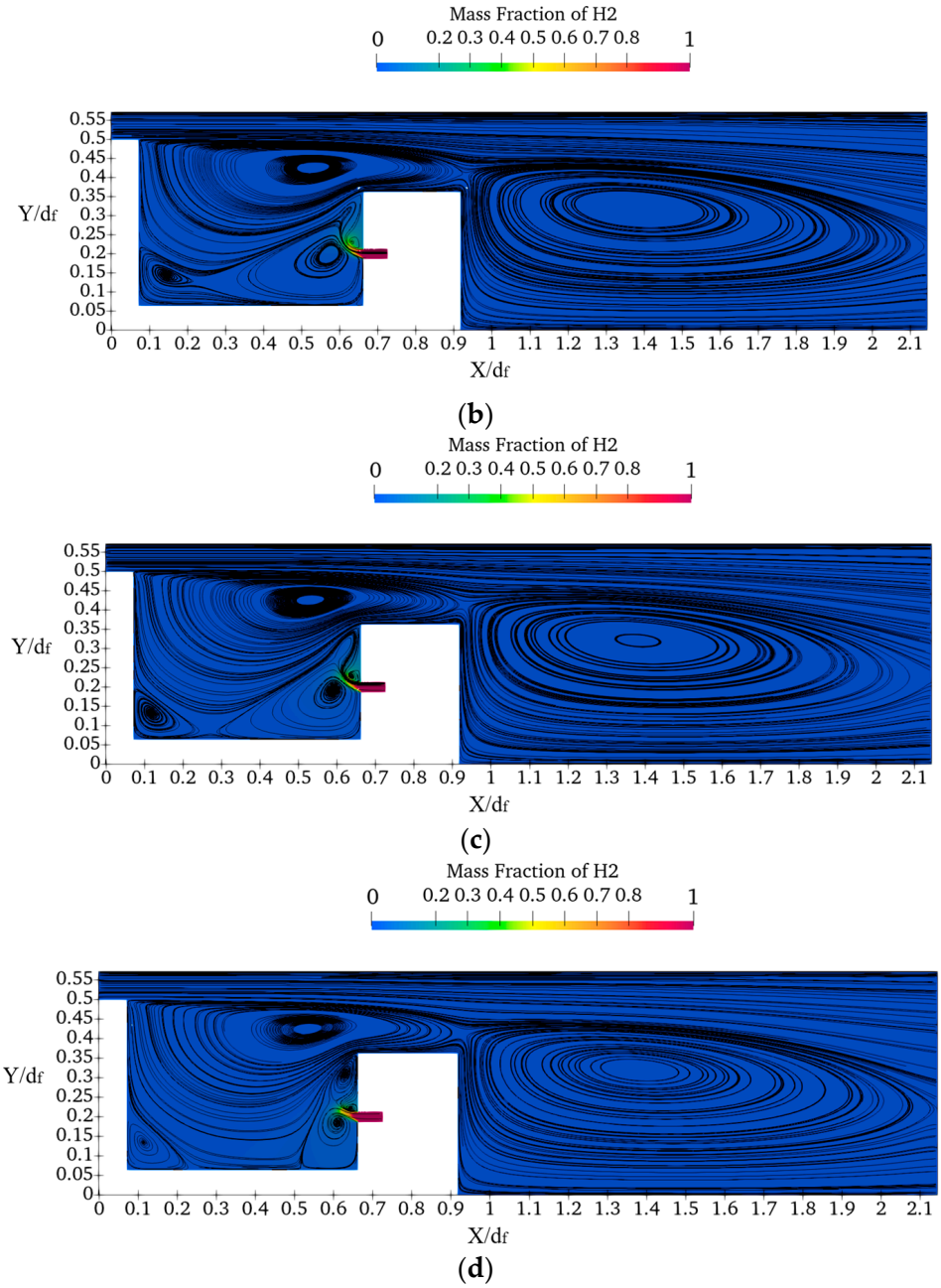

Figure 13. Mass fraction of hydrogen with streamlines under idle operating condition for (**a**) 0-degree, (**b**) 15-degree, (**c**) 30-degree and (**d**) 45-degree angles.

It was found that the 45-degree-angled air injectors showed superior mixing efficiency compared to the other transverse angle points for hydrogen fuel under the idle operating condition. The lowest mixing efficiency measured around fuel jets for the 45-degree transverse angle was 0.184, and the mixing efficiency was the highest inside the cavity for the 45-degree angle for all points. However, the 30-degree transverse angle mixing efficiency results for hydrogen were also acceptable and close to the 45-degree transverse angle results, with the lowest result of 0.207 shown around the fuel jets and the highest throughout the cavity.

Ammonia fuel was investigated using four different transverse angles under idle conditions (see Figure 14). The overall mixing efficiency was lower compared to propane, but the trend of the mixing efficiency was similar for these two fuels. Thee 45-degree transverse angle has the highest mixing efficiency over other transverse angles. However, in contrast to the hydrogen fuel, the mixing efficiency was the lowest for the 30-degree

angle around the fuel jets, at 0.236. Moreover, the 30-degree-angled air jets showed the second highest η_{mix} throughout the cavity. Since it is beneficial to have a lower η_{mix} around the fuel jets and higher values inside the cavity (3.1. Impact of Transverse Injection Angle for Propane under Idle and Low Power Conditions), it is suggested that 30-degree transverse-angled air jets are suitable for this application to improve mixing efficiency. Despite the fact that the 45-degree-angled air jets showed better results with hydrogen, the 30-degree-angled air jets showed better results for all three fuels.

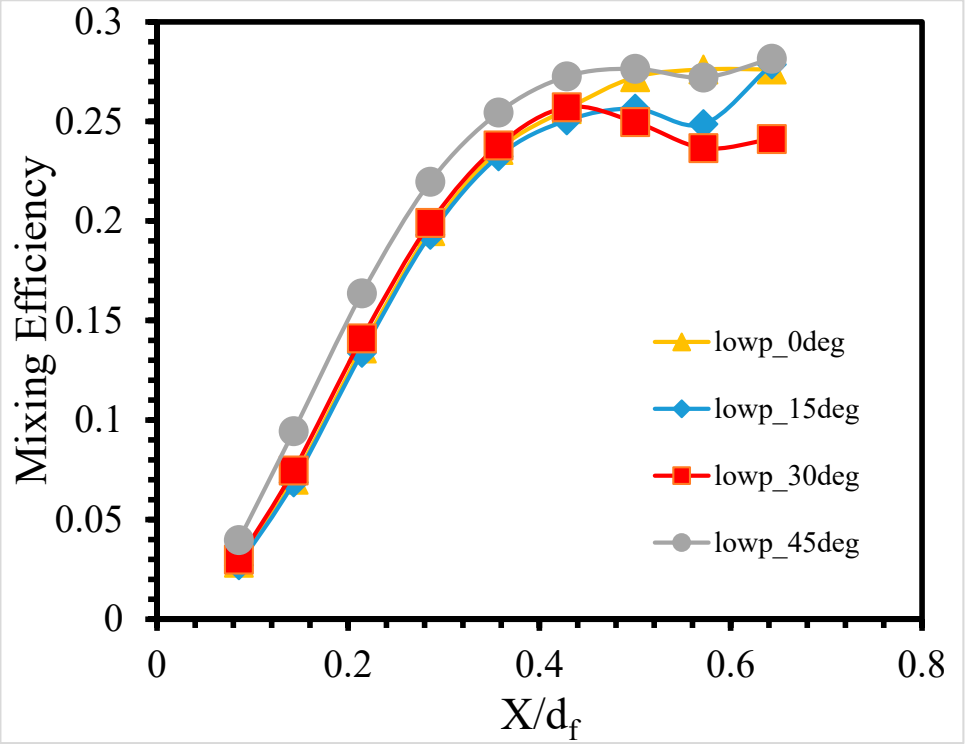

Figure 14. Mixing efficiency inside cavity for idle operating condition for ammonia.

Figure 15 shows the mass fraction of the ammonia and streamlines for the 0, 15-, 30- and 45-degree-angled air injectors. The fuel trajectory trend was similar to propane fuel. The trajectory of the fuel shifted to the bottom of the cavity for the 30-degree-angled air injectors. The fuel concentration was around 0.4 at the bottom of the cavity near the injectors for the 30-degree-angled air injector, whereas it was limited to 0.2 and 0.3 for the 0, 15- and 45-degree angles.

It is stated that the fuel trajectory behaviors of propane and ammonia are the same, moving towards the cavity bottom. On the other hand, the hydrogen fuel distribution tends to move to the top side of the cavity. Figures 16 and 17 clearly show that the fuel concentrations of ammonia and propane accumulate towards the bottom of the cavity. It also can be seen that the fuel concentration of propane was higher even at $X/d_f = 0.428$ than ammonia $X/d_f = 0.514$, which is the reason why the propane mixing efficiency was found to be higher than ammonia. When it comes to hydrogen fuel, Figure 18 shows that the hydrogen concentration moved upside of the cavity at $X/d_f = 0.642$, and the fuel concentration was very low beyond $X/d_f = 0.571$.

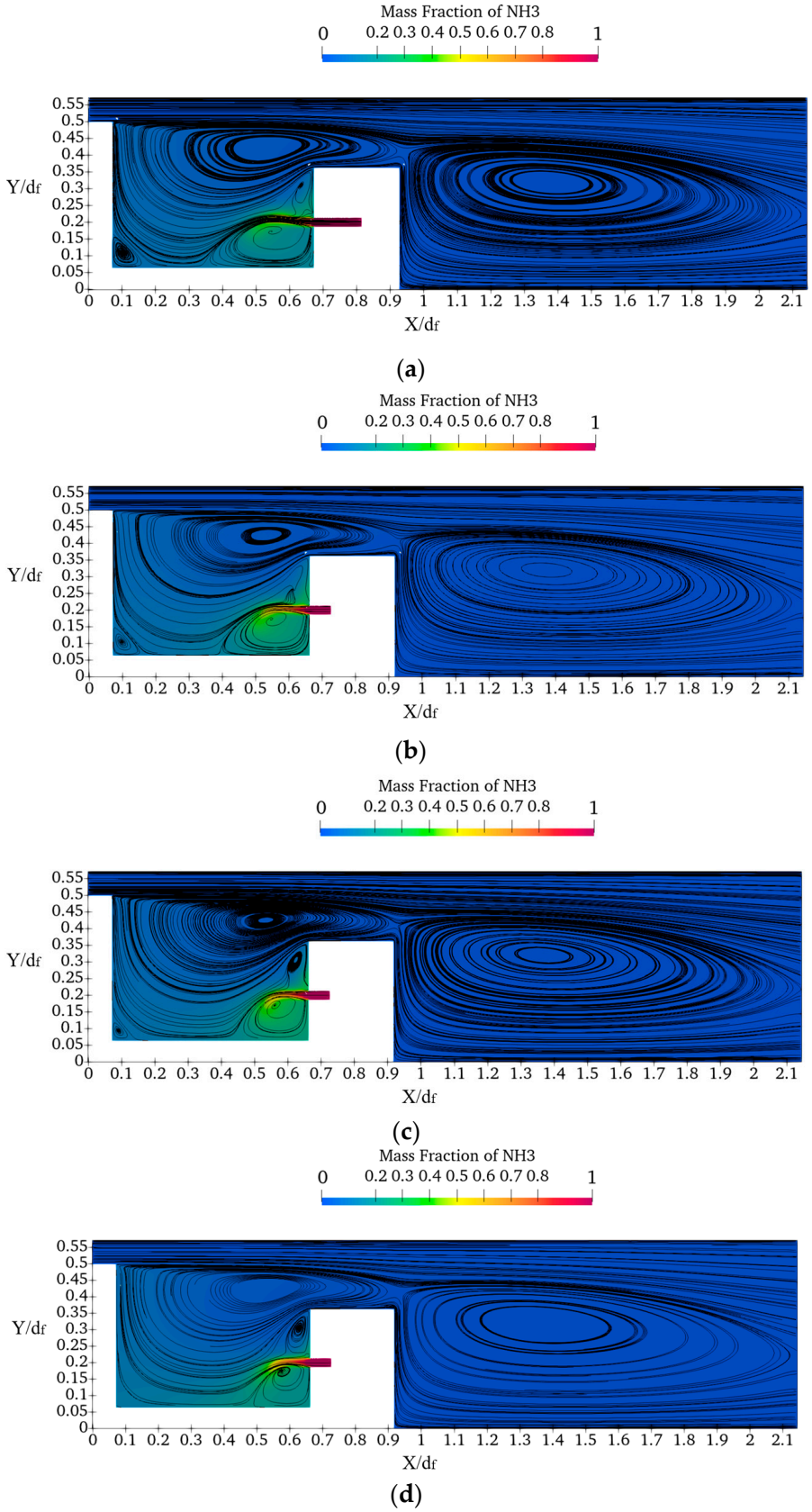

Figure 15. Mass fraction of ammonia with streamlines under idle operating condition for (**a**) 0-degree, (**b**) 15-degree, (**c**) 30-degree and (**d**) 45-degree angles.

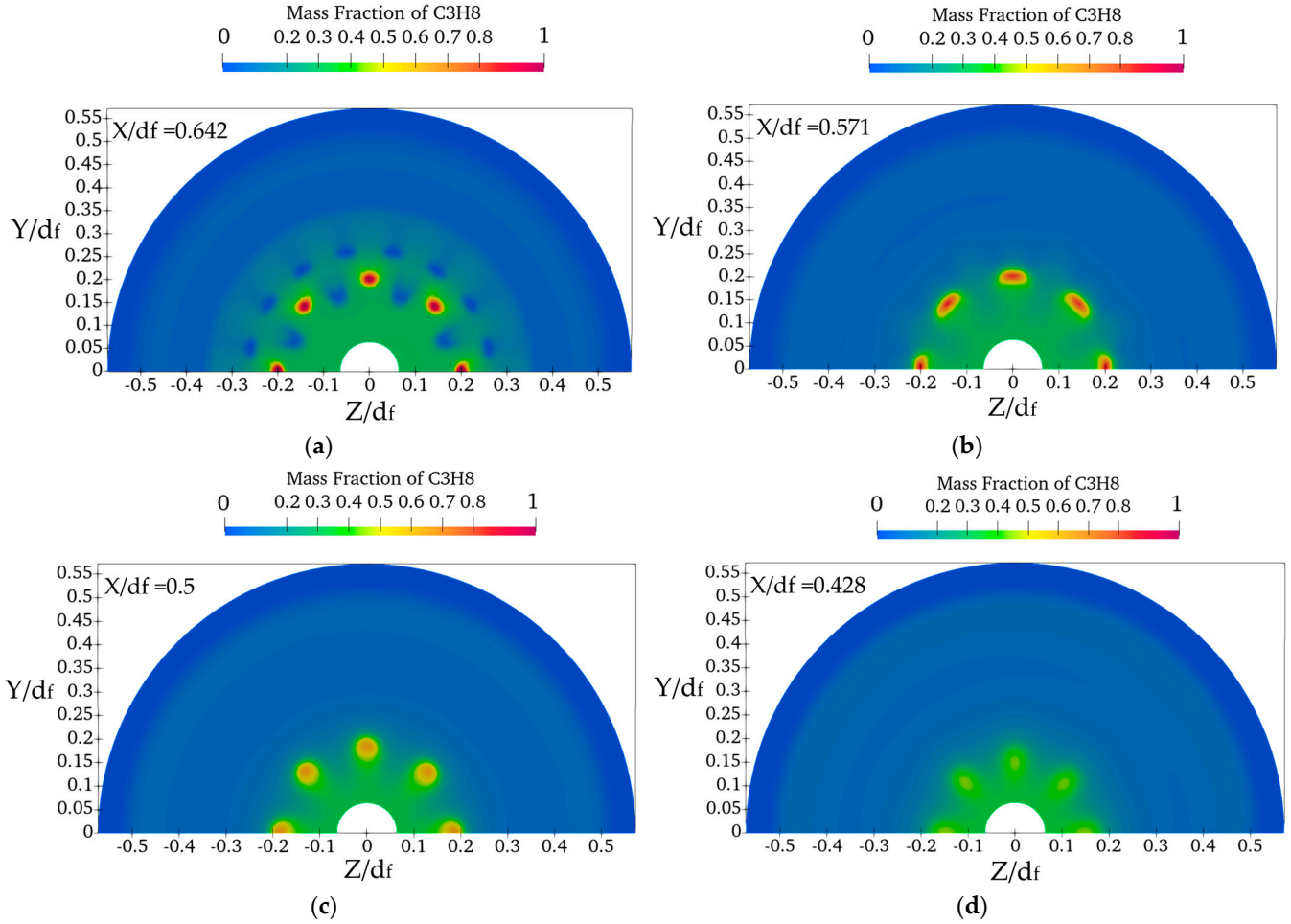

Figure 16. Mass fraction of propane for 30-degree transverse air injectors on Y-Z plane for (**a**) $X/d_f = 0.642$, (**b**) $X/d_f = 0.571$, (**c**) $X/d_f = 0.5$ and (**d**) $X/d_f = 0.428$ positions under idle condition.

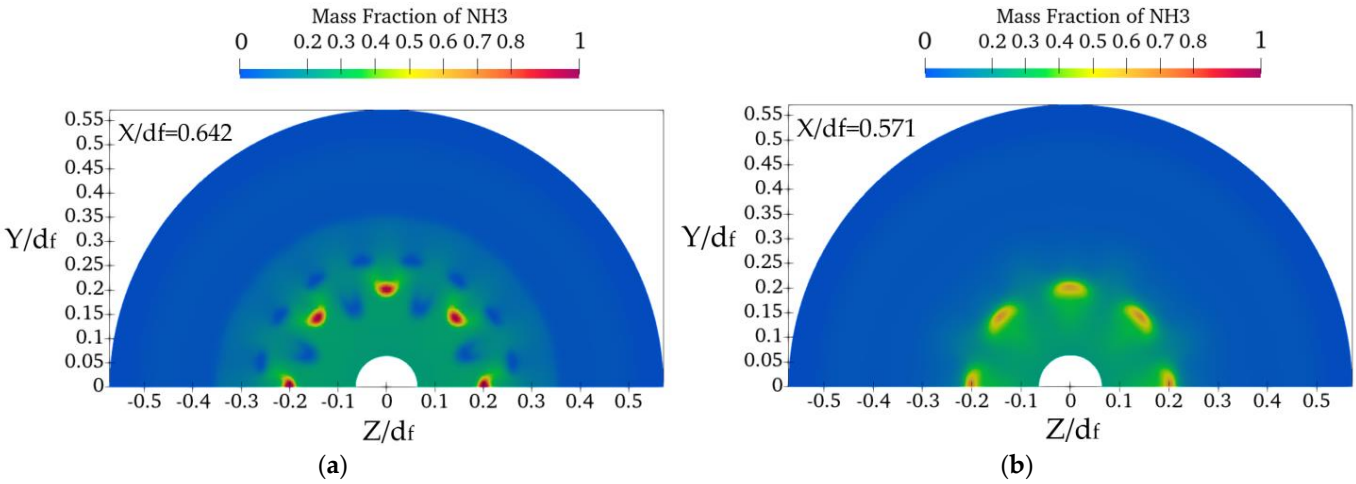

Figure 17. *Cont.*

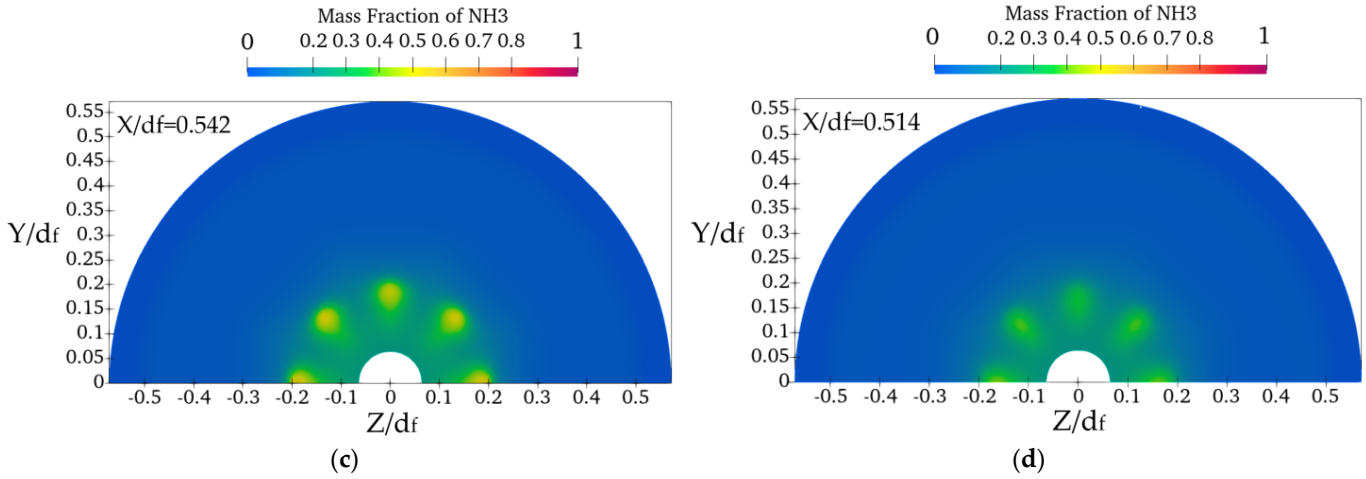

Figure 17. Mass fraction of ammonia for 30-degree transverse air injectors on Y-Z plane for (**a**) X/d_f = 0.642, (**b**) X/d_f = 0.571, (**c**) X/d_f = 0.542 and (**d**) X/d_f = 0.514 positions under idle condition.

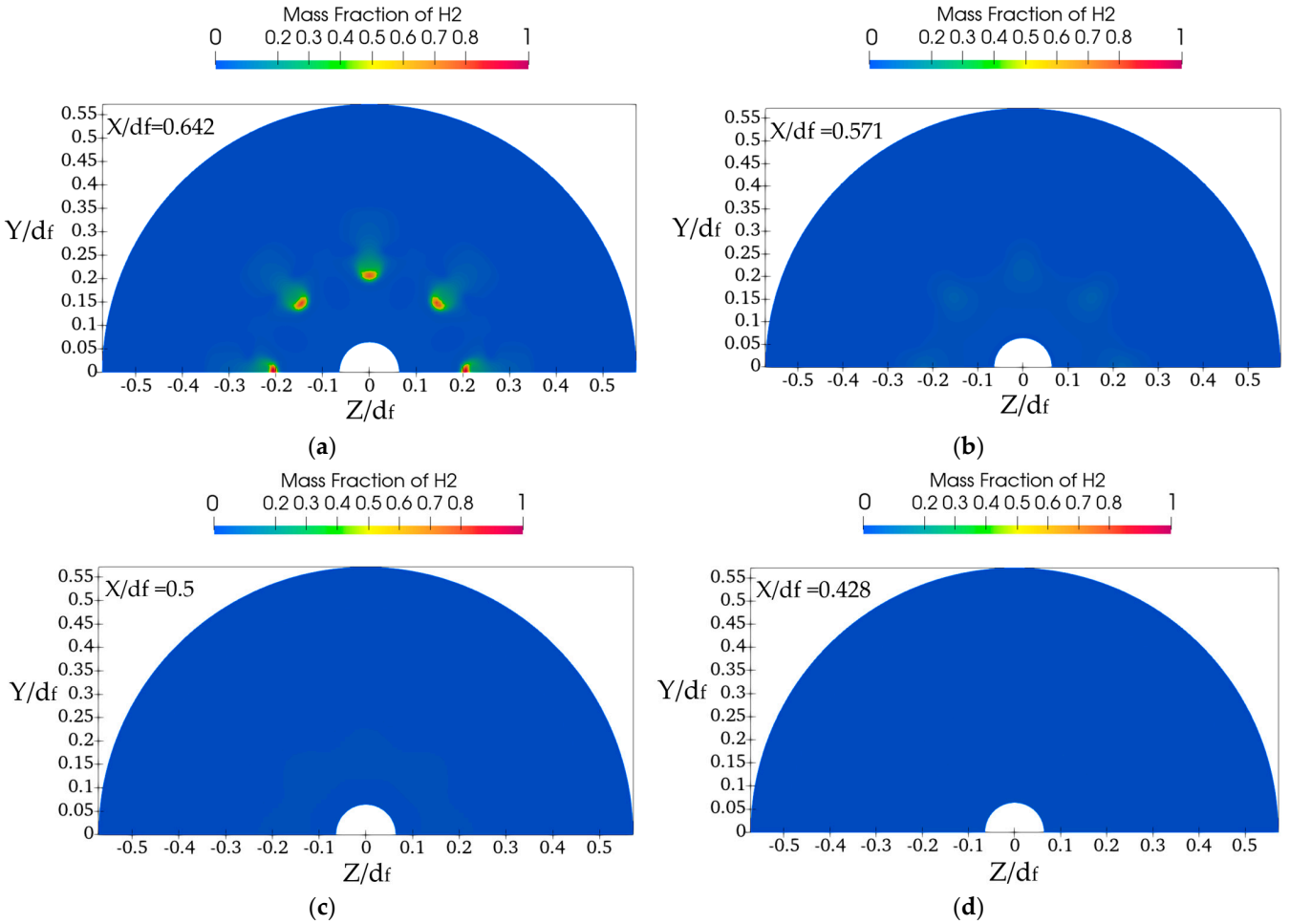

Figure 18. Mass fraction of hydrogen for 30-degree transverse air injectors on Y-Z plane for (**a**) X/df = 0.642, (**b**) X/df = 0.571, (**c**) X/df = 0.5 and (**d**) X/df = 0.428 positions under idle condition.

It can be said that propane and ammonia are more suitable for the current design of trapped-vortex combustors than hydrogen because hydrogen tends to diverge from the cavity center. Figure 19a,b illustrate that propane and ammonia move directly inside the cavity and accumulate at the center of the cavity around Z/d_f =0. However, it is clear that hydrogen moves upside of the cavity as soon as it enters the combustor, which suggests

that the usage of hydrogen in this configuration requires some alterations and design modifications of the combustor.

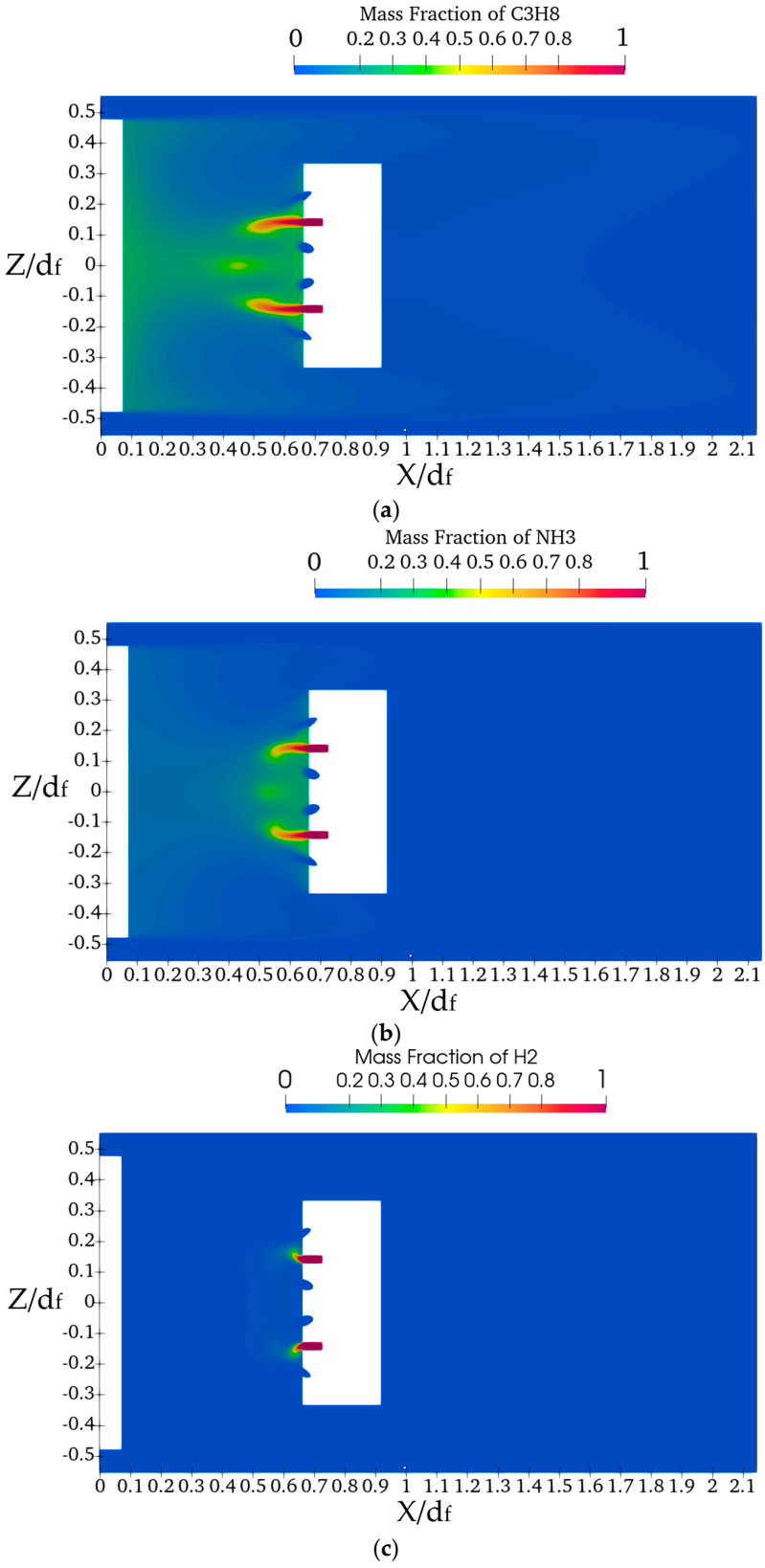

Figure 19. Mass fractions of (**a**) propane, (**b**) ammonia and (**c**) hydrogen for 30-degree transverse air injectors at X-Z plane for $Y/d_f = 0.142$ under idle condition.

4. Conclusions

The aim of this paper was to enhance the mixing of air and fuel in a trapped-vortex combustor for propane, hydrogen and ammonia. A numerical study was carried out for four different (0, 15, 30 and 45 degrees) air injectors to investigate the effect of the air injector angle on mixing efficiency. Propane fuel was also tested in the idle and low-power conditions to observe the behavior of the mixing as the operating conditions became more realistic, whereas hydrogen and ammonia were only tested in the idle condition. The following outcomes were induced from the present study:

(a) As the operating conditions approach realism, the mixing efficiency also increases, which suggests that the trapped-vortex combustor is suitable for operating under realistic conditions.
(b) The 45-degree- and 30-degree-angled air injectors have superior mixing throughout the cavity compared to the 0- and 15-degree angles for all three fuel types, with the 45-degree angle having slightly higher mixing efficiency overall.
(c) The 30-degree-angled fuel injector had the lowest mixing efficiency around the fuel injectors, which is important because this will lower the temperature around the fuel jets and reduce the possibility of damage to them, reducing the chance of fire reaching the fuel injectors. However, reacting simulations will require observation of this phenomenon.
(d) Propane and ammonia showed similar trends in terms of fuel injection trajectory trends. Fuel shifted towards the bottom of the cavity as the air injector angle increased, but a significant difference was observed on the 30-degree angled injector, where the fuel injection moved more towards the bottom of the cavity compared to the other angles.
(e) Hydrogen, on the other hand, had completely different injection behavior compared to the other two fuels. The fuel moved towards the upside of the cavity rather than moving into the cavity. A promising event was that as the air injector angle increased, the trajectory of the hydrogen moved towards the inside of the cavity. Even though this is positive, it suggests that hydrogen usage in trapped-vortex combustors requires some modification.

The present study provides valuable insights into the flow behavior and mass fraction of species, which are essential for assessing air–fuel mixing, especially for non-conventional fuels such as hydrogen and ammonia. A good validation of the numerical methodology is presented for a conventional fuel (propane). However, extensive experimental verification of the proposed mixing configurations for the novel fuel (hydrogen and ammonia) is required before commercializing the proposed concept. Future work involves constructing combustors and conducting experiments. In these experiments, fuel concentration inside the cavity can be measured with sensors to validate the mixing efficiency data, and the experiment could move on to igniting the fuel. Temperature distribution and species can be measured at the outlet of the combustor to evaluate combustion efficiency, pattern factors, and emissions. Moreover, the simulations could be performed by implementing large eddy simulations, and mixing efficiency could be enhanced by using different fuel arrangements. Furthermore, the combustion simulation could be carried out to observe the cavity flow behaviors under combustion conditions by implementing the Eddy Dissipation Model as well as combustion efficiency, pattern factor, and emissions.

Author Contributions: Conceptualization, S.M.D. and K.S.; methodology, S.M.D., K.S. and H.S.U.; software, H.S.U., K.S. and S.M.D.; validation, S.M.D. and K.S. and H.S.U.; formal analysis, H.S.U.; investigation, S.M.D. and K.S. and H.S.U.; resources, S.M.D.; data curation, H.S.U.; writing—original draft preparation, H.S.U.; writing—review and editing, S.M.D. and K.S.; visualization, H.S.U.; supervision, S.M.D. and K.S.; project administration, S.M.D.; All authors have read and agreed to the published version of the manuscript.

Funding: This research received no external funding other than the one listed in the acknowledgment section.

Data Availability Statement: The San Diego mechanism (date: 14 December 2016) with nitrogen chemistry (date: 23 July 2018) that was used in this paper can be found here: https://web.eng.ucsd.edu/mae/groups/combustion/mechanism.html (accessed on 25 January 2024).

Acknowledgments: Heval Serhat Uluk would like to thank his supervisors Sam Dakka and Kuldeep Singh. The author gratefully acknowledges a scholarship from The Republic of Turkey Ministry of National Education for their funding and support.

Conflicts of Interest: The authors declare no conflicts of interest.

Nomenclature

d_{aft}	Afterbody Diameter
d_c	Combustor Diameter
d_{ca}	Diameter of the Cavity Air Injector
d_f	Forebody Diameter
d_{fuel}	Fuel Injection Diameter
d_s	Spindle Diameter
g	Acceleration due to gravity
k	Turbulent Kinetic Energy (J)
L	Length of the Combustor
L_{air1}	Distance of Inner Cavity Air Injection
L_{air2}	Distance of Outer Cavity Air Injection
L_{ca}	Cavity Length
L_f	Distance of Fuel Injection
NO_x	Nitrogen Emission
P_r	Prandtl Number
S	Modulus of the mean rate-of-strain tensor
t_{aft}	Thickness of Afterbody
t_f	Thickness of Forebody
Greek	
G_b	Turbulence kinetic energy from buoyancy
G_k	Kinetic energy from mean velocity gradient
σ_{ij}	Stress tensor generated by molecular viscosity
S_k S_ε	Source Terms
μ_t	Turbulence viscosity
ν_T	Eddy viscosity
Y_M	Addition of fluctuating dilation in compressible turbulence to overall dissipation
Sc_t	Turbulent Schmidt Number
D_t	Turbulent Diffusivity
R_i	Production of species
S_i	Rate of creation by addition from the dispersed phase and user-defined sources
Y_i	Mass fraction of species
Abbreviation	
PISO	Pressure Implicit with Splitting of Operators
PRESTO	Pressure-Staggering Option
QUICK	Quadratic Upstream Interpolation for Convective Kinematics
RANS	Reynolds-Averaged Navier–Stokes
SST	Shear-Stress Transport
TVC	Trapped Vortex Combustor

References

1. Hsu, K.-Y.; Goss, L.P.; Trump, D.D.; Roquemore, W.M. Performance of a Trapped-Vortex Combustor. In Proceedings of the 33rd Aerospace Sciences Meeting and Exhibit, Reno, NV, USA, 9–12 January 1995.
2. Roquemore, W.M.; Shouse, D.; Burrus, D.; Johnson, A.; Cooper, C.; Duncart, B.; Hsu, K.-Y.; Katta, V.R.; Sturgess, G.J.; Vihineiv, I.; et al. Trapped Vortex Combustor Concept for Gas Turbine Engines. In Proceedings of the 39th Aerospace Sciences Meeting and Exhibit, Reno, NV, USA, 8–11 January 2001.

3. Lefebvre, A.H.; Ballal, D.R. *GAS Turbine Combustion: Alternative Fuels and Emissions*, 3rd ed.; CRC Press: Boca Raton, FL, USA, 2010.
4. Kumar, P.K.E.; Mishra, D.P. Numerical simulation of cavity flow structure in an axisymmetric trapped vortex combustor. *Aerosp. Sci. Technol.* **2012**, *21*, 16–23. [CrossRef]
5. Little, B.H.; Whipkey, R.R. Locked Vortex Afterbodies. *J. Aircr.* **1979**, *16*, 289–295. [CrossRef]
6. Mair, W.A. The Effect of a Rear-Mounted Disc on the Drag of a Blunt-Based Body of Revolution. *Aeronaut. Q.* **1965**, *16*, 350–360. [CrossRef]
7. Katta, V.R.; Roquemore, W.M. Numerical Studies On Trapped-Vortex Combustor. In Proceedings of the 32nd Joint Propulsion Conference and Exhibit, Lake Buena Vista, FL, USA, 1–3 July 1996.
8. Ghenai, C.; Zbeeb, K.; Janajreh, I. Combustion of alternative fuels in vortex trapped combustor. *Energy Convers. Manag.* **2013**, *65*, 819–828. [CrossRef]
9. Krishna, S.; Ravikrishna, R.V. Optical diagnostics of fuel-air mixing and vortex formation in a cavity combustor. *Exp. Therm. Fluid. Sci.* **2015**, *61*, 163–176. [CrossRef]
10. Singhal, A.; Ravikrishna, R.V. Single cavity trapped vortex combustor dynamics-Part-1: Experiments. *Sage J.* **2011**, *3*, 23–44. [CrossRef]
11. Sies, M.M.; Wahid, M.A. Numerical investigation of the asymmetrical vortex combustor running on biogas. *J. Adv. Res. Fluid. Mech. Therm. Sci.* **2020**, *74*, 1–18. [CrossRef]
12. Yan, P.; Fan, W.; Xu, H.; Zhang, R. Numerical Study of NOx Generation in a Trapped Vortex Combustor Fuelled by Kerosene Blended with Ethanol. *IOP Conf. Ser. Earth Environ. Sci.* **2021**, *721*, 012005. [CrossRef]
13. Cecere, D.; Giacomazzi, E.; Di Nardo, A.; Calchetti, G. Gas Turbine Combustion Technologies for Hydrogen Blends. *Energies* **2023**, *16*, 6829. [CrossRef]
14. Rizkalla, H.; Hernandez, F.; Bullard, T.; Benoit, J.; Stuttaford, P.; Thomassen, A. "Future-proofing" today's industrial gas turbines: Combustion system fuel flexibility improvements for hydrogen consumption in a renewable dominated marketplace. In Proceedings of the Future of Gas Turbine Technology, 9th International Gas Turbine Conference, Brussels, Belgium, 10–11 October 2018.
15. Sharifzadeh, R.; Afshari, A. Assessment of a hydrogen-fueled swirling trapped-vortex combustor using large-eddy simulation. *Fuel* **2024**, *357*, 129847. [CrossRef]
16. Guo, Y.; Gong, C.; Huang, Y.; Duan, F.; He, X. Combustion and emission performance of swirling-flow single trapped vortex combustor. *Appl. Therm. Eng.* **2024**, *236*, 121678. [CrossRef]
17. Zhang, J.; Wang, M.; Wang, L.; Wang, J.; Jiang, P.; He, X. Experimental Investigation on Liner Cooling Characteristics of a Mixed-Flow Trapped Vortex Combustor. *J. Therm. Sci.* **2023**, *32*, 2222–2234. [CrossRef]
18. Jiang, P.; Xiong, S.; Xu, W.; Du, Z.; He, X. Experimental study on the influence of inlet velocity and fuel/air ratio on outlet temperature profile performance in a turboshaft engine combustor. *Fuel* **2024**, *357*, 129715. [CrossRef]
19. Kang, Y.; Wang, C.; Fang, G.; Xing, F.; Chan, S. Flow and Combustion Characteristics of Wave Rotor–Trapped Vortex Combustor System. *Energies* **2023**, *16*, 326. [CrossRef]
20. Jeong, S.M.; Han, H.S.; Sung, B.K.; Kim, W.; Choi, J.Y. Reactive Flow Dynamics of Low-Frequency Instability in a Scramjet Combustor. *Aerospace* **2023**, *10*, 932. [CrossRef]
21. Uluk, H.S.; Dakka, S.; Singh, K.; Jefferson-Loveday, R. Non-reacting Numerical Simulation of Axisymmetric Trapped Vortex Combustor. In Proceedings of the ICAAAE 2023: XVII. International Conference on Aeronautical and Aerospace Engineering, London, UK, 11–12 December 2023.
22. Ansys Fluent Theory Guide. 2022. Available online: http://www.ansys.com (accessed on 12 February 2024).
23. Feng, Y.; Li, X.; Ren, X.; Gu, C.; Lv, X.; Li, S.; Wang, Z. Experimental and Numerical Investigation of the Non-Reacting Flow in a High-Fidelity Heavy-Duty Gas Turbine DLN Combustor. *Energies* **2022**, *15*, 9551. [CrossRef]
24. Fąfara, J.M.; Modliński, N. Computational Fluid Dynamics (CFD) Assessment of the Internal Flue Gases Recirculation (IFGR) Applied to Gas Microturbine in the Context of More Hydrogen-Enriched Fuel Use. *Energies* **2023**, *16*, 6703. [CrossRef]
25. Benim, A.C.; Canal, C.D.; Boke, Y.E. A validation study for rans based modelling of swirling pulverized fuel flames. *Energies* **2021**, *14*, 7323. [CrossRef]
26. Li, Z.; Liu, Z.; Chen, P.; Liu, J.; Wu, J. Numerical Comparative Study of Fuel Cavitation in Microchannels under Different Turbulence Models. *Energies* **2022**, *15*, 8265. [CrossRef]
27. Lin, J.; Li, H.; Zhang, Y.; Yang, J. Experimental and Numerical Study of a Two-Stage Swirl Burner. *Energies* **2022**, *15*, 1097. [CrossRef]
28. Cao, C.; Gao, Y.; Wang, S.; Liu, F.; Liu, C.; Mu, Y.; Mei, D.; Xu, G. Numerical Investigation on Mechanism of Swirling Flow of the Prefilming Air-Blast Fuel Injector. *Energies* **2023**, *16*, 650. [CrossRef]
29. Liu, S.; Zhao, N.; Zhang, J.; Yang, J.; Li, Z.; Zheng, H. Experimental and numerical investigations of plasma ignition characteristics in gas turbine combustors. *Energies* **2019**, *12*, 1511. [CrossRef]
30. Wang, K.; Li, F.; Zhou, T.; Ao, Y. Numerical Study of Combustion and Emission Characteristics for Hydrogen Mixed Fuel in the Methane-Fueled Gas Turbine Combustor. *Aerospace* **2023**, *10*, 72. [CrossRef]
31. Lim, J.T.; Ng, E.Y.-K.; Saeedipour, H.; Lee, H.K. Numerical Simulation of Effective Heat Recapture Ammonia Pyrolysis System for Hydrogen Energy. *Inventions* **2024**, *9*, 56. [CrossRef]

32. Hu, G.; Qin, Q.; Jin, W.; Li, J. Large Eddy Simulation of the Influences of the Pilot-Stage Structure on the Flow Characteristics in a Centrally Staged High-Temperature-Rise Combustor. *Aerospace* **2022**, *9*, 782. [CrossRef]
33. Liu, Y.-Y.; Li, R.-M.; He-Xia, L.; Mao-Lin, Y. Effects of Fuelling Scheme on the Performance of a Trapped Vortex Combustor Rig. In Proceedings of the 45th AIAA/ASME/SAE/ASEE Joint Propulsion Conference & Exhibit, Denver, CO, USA, 2–5 August 2009.
34. Carusotto, S.; Goel, P.; Baratta, M.; Misul, D.A.; Salvadori, S.; Cardile, F.; Forno, L.; Toppino, M.; Valsania, M. Combustion Characterization in a Diffusive Gas Turbine Burner for Hydrogen-Compliant Applications. *Energies* **2022**, *15*, 4117. [CrossRef]
35. Farisco, F.; Castellanos, L.; Woisetschläger, J.; Sanz, W. Numerical steady and transient evaluation of a confined swirl stabilized burner. *Int. J. Turbomach. Propuls. Power* **2021**, *6*, 46. [CrossRef]
36. Chemical-Kinetic Mechanisms for Combustion Applications. San Diego Mechanism Web Page, Mechanical and Aerospace Engineering (Combustion Research), University of California at San Diego. 2024, Volume 5. Available online: http://combustion.ucsd.edu (accessed on 25 January 2024).
37. Celik, I.B.; Li, J. Assessment of numerical uncertainty for the calculations of turbulent tow over a backward-facing step. *Int. J. Numer. Meth. Fluids* **2005**, *49*, 1015–1031. [CrossRef]
38. Sundararaj, R.H.; Kumar, R.D.; Raut, A.K.; Sekar, T.C.; Pandey, V.; Kushari, A.; Puri, S.K. Combustion and emission characteristics from biojet fuel blends in a gas turbine combustor. *Energy* **2019**, *182*, 689–705. [CrossRef]
39. Gerdroodbary, M.B.; Fallah, K.; Pourmirzaagha, H. Characteristics of transverse hydrogen jet in presence of multi air jets within scramjet combustor. *Acta Astronaut.* **2017**, *132*, 25–32. [CrossRef]